A dynamic coarsening approach to immiscible multiphase flows in heterogeneous porous media

Narges Dashtbesh, Guillaume Enchéry, Benoît Noetinger

A dynamic coarsening approach to immiscible multiphase flows in heterogeneous porous media.

1 Introduction

Numerical modelling is a major tool in applied geoscience for optimizing prospect exploitation at minimal risks and cost while accounting for more and more strict environmental constraints (Suslick and Schiozer, 2004). Efficient and accurate modelling of immiscible flows in heterogeneous porous media is important in many fields of application including oil recovery, waste storage (Nuclear or CO_2), hydrogeology for contaminant remedial purposes, geothermal energy recovery, and other energy-related processes. One of the main challenges related to flow modelling in porous media is the heterogeneity of the rock properties which can vary over several orders of magnitude and many length scales, from pore to reservoir scale. It is well-known that the fine-scale heterogeneity, implying strong localization or channelling of the flow can change field-scale processes, leading to early breakthrough or poor recovery that can hinder the global profitability of an EOR project (Tayari et al., 2018). To capture the influence of the medium heterogeneity, the geological models which describe the reservoir rock properties, are generated at high spatial resolutions. Statistical methods are implemented to propagate the few measured seismic/well/outcrop data to the whole domain, resulting in high uncertainties that must be quantified too. Then the engineer must propagate the uncertainties on the output data of interest, such as hydrocarbons recovery, to recommend the best decisions (Abdul Hamid and Muggeridge, 2018). These models, generally, include several equally probable realizations of the same reservoir. Solving multi-phase flow equations on these high-resolution grids of millions of cells is not computationally efficient. Even with high computing power, it is necessary to run several simulations on different independent realizations, as carrying out a single simulation on a highly detailed geological model is not sufficient. Thus upscaling, the process of propagating the properties from a high-resolution model to a model with less resolution, remains necessary whatever the available computing resources are. The important aim of any upscaling method is to capture the effect of small-scale heterogeneities in an averaged sense, with well-controlled loss of information. While additive rock properties, like porosity, may be upscaled using the direct arithmetic averaging, upscaling the permeability and transmissibility is not straightforward due to the non-linear dependence on the fine-scale properties. The situation is far more complex when considering multiphase flows, due to the strong coupling between pressure and saturation equations that are the basis of the viscous fingering mechanism (Ganjeh-Ghazvini, 2019). Coarse scale equations may be different from their fine-scale counterpart, leading to major changes in the simulation workflow.

In single-phase flow, there exist different criteria for the classification of upscaling methods, from analytical averaging methods versus numerical flow-based methods, to local versus extended local and global methods. For example, in local methods, the upscaled permeability in each coarse grid block is solely restricted to the effect of the underlying permeability within the grid block. In extended local upscaling methods, the computation region is extended to include a buffer zone, and in global methods, a fine-scale solution is used to compute the upscaled properties. Extensive reviews may be found in the works of Durlofsky (1991), Renard and Marsily (1997), Wu et al. (2002), Farmer (2002), Mourlanette et al. (2020), and Colecchio et al. (2020). There is no mathematical foundation to analyse the quality and accuracy of the upscaling method, and the closest assessment we can reach is to compare the upscaled solutions with a reference base fine solution (Correia et al., 2018; Darban et al., 2020; Preux, 2016; Preux et al., 2016). The challenge in upscaling becomes even more critical in multi-phase processes. The upscaling of absolute permeability, or single-phase upscaling, alone cannot model a multi-phase process and may lead to incorrect oil recovery and water breakthrough times in reservoir simulations. Upscaling of relative permeability, or multiphase upscaling, has been the subject of many articles, but there are practical difficulties in this type of upscaling, no matter what method is used (Barker and Dupouy, 1999; Barker and Thibeau, 1997; Christie, 1996; Darman et al., 2002). The difficulty with the classical methods of multi-phase upscaling, like pseudo-functions, is that they mix averaging with numerical discretization issues (Artus et al., 2004; Noetinger et al., 2004). The net result is an unclear mix of techniques that is over-amplified by the nonlinear character of the underlying equations, typically the so-called pressure equation coupled with the saturation transport equation. These issues are extensively discussed in the mentioned articles.

Another challenge in multiphase flow simulations arises from the discretization of the governing equations. A desirable discretization method should be accurate, stable, and locally conservative to respect the physical process. Another important feature is the computational efficiency. Low-order methods such as finite volume methods (FV) are currently widely used for solving these equations. They are stable, mass conservative, and computationally efficient. To improve the accuracy of the approximating solution, especially in the presence of highly heterogeneous anisotropic media, there has been a great interest in high order discontinuous Galerkin (DG) methods over the last two decades. The main idea of DG methods, first introduced by Reed and Hill (1973), consists in approximating the solution using discontinuous polynomials localized in each element and a weakly enforcement of continuity between the elements. It has gone through massive developments leading to different formulations of DG methods. The mathematical aspects of DG methods are detailed in the books of Riviere (2008) and Di Pietro and Ern (2011).

DG methods are like finite element methods but with discontinuities in test functions. DG methods can also be viewed like finite volume methods, in terms of element-wise approximating functions. But, in DG methods, the solution is generally approximated by a polynomial of degree greater than one and not by piece-wise constant functions like in finite volume methods. We may say that DG methods incorporate the favourable features of finite volume and finite element methods. They are highly parallelizable, flexible in using variable polynomial degrees in different elements, and locally conservative. These important properties made them popular in many fields of applications including flow and transport in porous media. Many researchers have applied discontinuous Galerkin methods for single and multiphase flow problems of reservoir simulations, from the early work of Riviere et al. (2000), where the DG method was applied to a single-phase problem in porous media, to the works of Riviere and Wheeler (2002), Bastian and Riviere (2004), Ern et al. (2010), Bastian (2014), Cappanera and Riviere (2019), and Fabien et al. (2020) for multiphase flows, to name a few. However, DG methods suffer from one main drawback, which is the increase in the number of degrees of freedom, and ultimately the increase in computational time compared to other numerical methods.

Besides adopting higher-order discretization methods, adaptive use of higher resolution grids in some parts of the domain is another approach to improve the accuracy of solutions. The idea of adaptive gridding through local spatial refinement goes back to the 1980s in reservoir simulations (Han et al., 1987; Quandalle, 1983; Schmidt and Jacobs, 1988). Conversely, nonuniform coarsening methods can also be adaptively applied to reduce spatial resolution according to specific flow features. The agglomeration approaches have many advantageous especially compared to local mesh refinement thanks to the availability of the fine geological model and have been addressed in several works (Ashjari et al., 2007; Durlofsky et al., 1997; Hauge et al., 2012; Li, 1995).

The purpose of this study is to propose an efficient and accurate approach that avoids the challenges of multiphase upscaling and maintains a high order of accuracy in the whole domain. To reach this aim, we have developed a scheme to treat different flow regions separately. Considering a two-phase flow process, like a waterflood in an oil reservoir, there is an interface between the bulk of water and oil. Near the front, the interaction of viscous fingering and heterogeneity of porous medium is important to be captured for industrial applications (Abdul Hamid and Muggeridge, 2018). Like in Hauge et al. (2012), we use adaptive coarsening outside the two-phase flow region to concentrate the calculation efforts within the front area. As a result, the use of any multiphase upscaling technique is avoided. The finite volume method in this high-resolution region gives satisfactory results in a computationally efficient way. Far from the front, in single-phase areas, the grid is coarsened, and a linear DG scheme is used to get more accurate total fluxes. To be able to apply different strategies in different regions, an estimation of the location of the saturation discontinuity is needed. There are different fast approaches for interface modelling. Streamline methods are developed as an alternative to common simulation techniques and work based on the reduction of the main transport problem into a series of 1D problems along streamlines (Datta-Gupta and King, 2007). Another approach to track the evolution of interfaces is the Fast Marching Method (FMM), an approach to solving the Eikonal equation very close to Dijkstra's method (Sethian, 1996). In this study, we present a new technique to estimate the position of

the saturation discontinuity. The objective of this method is to approximately track the position of the front, without solving the fully-coupled pressure and saturation equations on the whole grid.

The paper is organized as follows. We detail the formulation and implementation of the proposed algorithm in the first section and then discuss its advantages and limitations through numerical examples.

2 Driving equations

In this paper, we consider an immiscible two-phase flow model, for example, water and oil in a waterflood problem in a porous medium. When modelling the behaviour of fluids flowing in porous media, mass conservation and Darcy's law are used to derive the system of equations. Considering the fluids to be incompressible, the conservation equation for each phase is,

$$\phi \frac{\partial s_\alpha}{\partial t} + \nabla.(\boldsymbol{\nu}_\alpha) = q_\alpha, \qquad \alpha = o, w \qquad \text{Eq. 1}$$

where s_α is the phase saturation, $\boldsymbol{\nu}_\alpha$ is the phase velocity, q_α is the source term, and ϕ is the rock porosity. Darcy's law for the phase velocity, in the absence of gravitational and capillary forces, reads,

$$\boldsymbol{\nu}_\alpha = -\frac{k k_{r_\alpha}(s_\alpha)}{\mu_\alpha} \nabla p \qquad \text{Eq. 2}$$

with p the local pressure which is equal to water and oil pressure in our case, k the absolute permeability, μ_α the viscosity of each phase, and k_{r_α} the relative permeability of each phase, usually defined as a function of saturation. In the numerical examples, throughout this paper, we use a quadratic relationship, that reads in terms of reduced water saturation, $s_w^* = \frac{s_w - s_{w_i}}{1 - s_{w_i} - s_{o_r}}$: $k_{r_w} = (s_w^*)^2$ and $k_{r_o} = (1 - s_w^*)^2$. k_{r_α}/μ_α is called the phase mobility and is denoted by λ_α. Adding both conservation equations and considering that $s_w + s_o = 1$ gives,

$$\nabla.\boldsymbol{\nu} = q \qquad \text{Eq. 3}$$

with $\boldsymbol{\nu}$ the total velocity or the sum of water and oil velocities, and q the total source term. Writing Darcy's law for the total velocity gives,

$$\boldsymbol{\nu} = -k\lambda_T \nabla p \qquad \text{Eq. 4}$$

where λ_T is the total mobility, the sum of water and oil mobilities:

$$\lambda_T = \lambda_w + \lambda_o = \frac{k_{r_w}(s_w)}{\mu_w} + \frac{k_{r_o}(s_o)}{\mu_o} \qquad \text{Eq. 5}$$

A substitution of total Darcy's law into the overall mass-conservation law gives the 'pressure equation':

$$-\nabla.(k\lambda_T(s_w)\nabla p) = q \qquad \text{Eq. 6}$$

To close the model, boundary conditions are imposed:

$$\begin{cases} p = p_D, & on\ \partial\Omega_D \\ \boldsymbol{\nu}.\boldsymbol{n} = 0, & on\ \partial\Omega_N \end{cases} \qquad \text{Eq. 7}$$

which correspond to Dirichlet and homogeneous Neumann boundary conditions on the boundaries of the reservoir domain. $\boldsymbol{n}$ is the outward unit normal on these boundaries.

Writing the conservation equation of water in terms of total velocity $\boldsymbol{v}$ and water fractional flow f_w leads to the 'saturation equation':

$$\phi \frac{\partial s_w}{\partial t} + \nabla . (f_w(s_w)\boldsymbol{v}) = q_w \qquad \text{Eq. 8}$$

to be solved with the initial and boundary conditions:

$$\begin{cases} s_w = s_w^0, & in\ \Omega \\ s_w = s_D, & if\ \boldsymbol{v}.\boldsymbol{n} < 0\ \ on \partial\Omega \end{cases} \qquad \text{Eq. 9}$$

The system of equations described through Eq. 6 to Eq. 9 is nonlinearly coupled. The coupling arises via the saturation dependant mobilities in the pressure equation and pressure dependent velocities in the saturation equation. One common approach for solving this coupled system of equations is the sequential approach. This approach aims at solving the pressure and saturation separately and sequentially. The main advantage lies in the reduction of the size of the linear systems to be solved. Another benefit of this approach is that we can mix different discretization methods in the same system.

3 Numerical solution methods

3.1 Finite Volume discretization for the pressure equation

We assume the reservoir domain Ω, with boundary $\partial\Omega$, is partitioned into cells Ω_i. The standard finite-volume two-point flux approximation to discretize the pressure equation gives:

$$\sum_j v_{ij}^{n+1} = \sum_j T_{ij}^n \left(p_i^{n+1} - p_j^{n+1}\right) = q_i^{n+1}, \ \ \forall \Omega_i \in \Omega \qquad \text{Eq. 10}$$

Where the superscripts n and $n+1$ represent the time step, $p^{n+1} = \left\{p_i^{n+1}\right\}$ is the new cell-wise constant approximated pressure, q_i^{n+1} is the volume average of the total source term q over the cell i at timestep $n+1$, and T_{ij}^n is the face transmissibility given by the distance-weighted harmonic average of $k\lambda_T^n$ values in the two neighbouring cells Ω_i and Ω_j:

$$T_{ij}^n = \left|\sigma_{ij}\right| \left(\frac{d_{i,\sigma}}{k_i \lambda_{T\,i}^n} + \frac{d_{j,\sigma}}{k_j \lambda_{T\,j}^n} \right)^{-1} \qquad \text{Eq. 11}$$

$\left|\sigma_{ij}\right|$ is the area of the face $\sigma_{ij} = \partial\Omega_i \cap \partial\Omega_j$, $d_{i,\sigma}$ and $d_{j,\sigma}$ denote the distance from respective cell centres to the centre of the face σ_{ij}.The transmissibility depends on time through its implicit dependence on the local saturation at time t^n.

3.2 Finite Volume discretization for the saturation equation

The implicit scheme for solving the saturation equation is,

$$\phi_i |\Omega_i| \frac{s_i^{n+1} - s_i^n}{\Delta t} + \sum_{j \neq i} \left[f_w\left(s_{ij}^{n+1}\right) v_{ij}^{n+1} \right] = q_i^{n+1} \qquad \text{Eq. 12}$$

where ϕ_i is the porosity of cell i, $|\Omega_i|$ is the volume of cell i, Δt is the time step, v_{ij}^{n+1} is the total flux coming from the solution of the pressure equation, and $f_w\left(s_{ij}^{n+1}\right)$ denotes the fractional-flow function associated with the face σ_{ij}. $f_w\left(s_{ij}^{n+1}\right)$ is chosen using the upwind scheme,

$$f_w(s_{ij}^{n+1}) = \begin{cases} f_w\left(s_i^{n+1}\right), & if\ v_{ij} \geq 0, \\ f_w\left(s_j^{n+1}\right), & if\ v_{ij} < 0. \end{cases} \qquad \text{Eq. 13}$$

3.3 Discontinuous Galerkin discretization for the pressure equation:

To obtain the DG discretization of the pressure equation, Eq. 6 and Eq. 7, we first re-write the elliptic pressure equation in a mixed form through the introduction of an auxiliary variable $\boldsymbol{z} := -\nabla p$ (Frank et al., 2015),

$$\begin{cases} \boldsymbol{z} = -\nabla p, & in\ \Omega, \\ \nabla.(k\lambda_T \boldsymbol{z}) = q, & in\ \Omega, \\ p = p_D, & on\ \partial\Omega_D, \\ \boldsymbol{z}.\boldsymbol{n} = 0, & on\ \partial\Omega_N. \end{cases} \qquad \text{Eq. 14}$$

By multiplying the first and second equations by smooth test functions $\boldsymbol{y}$ and ω, respectively, and integrating by part on a cell Ω_i we get,

$$\int_{\Omega_i} \boldsymbol{y}.\boldsymbol{z} - \int_{\Omega_i} \nabla.\boldsymbol{y}p + \int_{\partial\Omega_i} \boldsymbol{y}.\boldsymbol{n}p = 0, \qquad \text{Eq. 15}$$

$$-\int_{\Omega_i} \nabla\omega.(k\lambda_T \boldsymbol{z}) + \int_{\partial\Omega_i} \omega k\lambda_T \boldsymbol{z}.\boldsymbol{n} = \int_{\Omega_i} \omega q. \qquad \text{Eq. 16}$$

For the numerical resolution of Eq. 15 and Eq. 16, we use FESTUNG[1], the Finite Element Simulation Toolbox for Unstructured Grids, an open-source MATLAB/GNU Octave toolbox, developed as a package for discontinuous Galerkin methods. For more details of this DG method and its implementation, the reader can refer to the series of papers that the authors of this toolbox have published: Frank et al. (2015), Reuter et al. (2016), Jaust et al. (2018), Reuter et al. (2018), and Reuter et al. (2020). Let us denote by $\mathbb{P}_P(\Omega_i)$ the space of polynomials of degree at most P on $\Omega_i \in \Omega$ and by $\mathbb{P}_P(\Omega) = \{\omega_i : \bar{\Omega} \to \mathbb{R};\ \forall \Omega_i \in \Omega, \omega_i|\Omega_i \in \mathbb{P}_P(\Omega_i)\}$ the space of discontinuous polynomials on the partitioned domain Ω. The DG method is used to solve the following system to obtain $p_i^{n+1} \in P_P(\Omega)$ and $\boldsymbol{z}_i^{n+1} \in [P_P(\Omega)]^2$, for $\forall \Omega_i \in \Omega$, $\forall \mathbf{y}_i \in [P_P(\Omega)]^2$, and $\forall \omega_i \in P_P(\Omega)$:

$$\int_{\Omega_i} \boldsymbol{y}_i.\boldsymbol{z}_i^{n+1} - \int_{\Omega_i} \nabla.\boldsymbol{y}_i p_i^{n+1} + \sum_j \int_{\sigma_{ij}} \boldsymbol{y}_i.\boldsymbol{n}_{ij} \begin{cases} \{p_i^{n+1}\}, & on\ \varepsilon_\Omega \\ p_D, & on\ \varepsilon_D = 0, \\ p_i^{n+1}, & on\ \varepsilon_N \end{cases} \qquad \text{Eq. 17}$$

[1] https://github.com/festung/FESTUNG

$$
\begin{aligned}
&-\int_{\Omega_i} \nabla\omega_i.\left(k_i\lambda_{T_i}^n \boldsymbol{z}_i^{n+1}\right) \\
&+\sum_j \int_{\sigma_{ij}} \omega_i \begin{cases} \left\{\left(k_i\lambda_{T_i}^n\right)\boldsymbol{z}_i^{n+1}\right\}.\boldsymbol{n}_{ij} + \dfrac{\eta\gamma_{ij}^n}{h_{ij}}[\![p_i^{n+1}]\!].\boldsymbol{n}_{ij}, & on\ \varepsilon_\Omega \\ \left(k_i\lambda_{T_i}^n\right)\boldsymbol{z}_i^{n+1}.\boldsymbol{n}_{ij} + \dfrac{\eta\gamma_{ij}^n}{h_{ij}}\left(p_i^{n+1} - p_D\right), & on\ \varepsilon_D \\ 0, & on\ \varepsilon_N \end{cases} \\
&= \int_{\Omega_i} \omega_i q_i^{n+1}
\end{aligned}
\qquad \text{Eq. 18}
$$

where η is a penalty coefficient, and h_{ij} is the diameter of the face σ_{ij}. ε_Ω, ε_D, and ε_N denote the set of interior faces, Dirichlet and Neumann boundaries, respectively (Frank et al., 2015). For any interior face σ_{ij} and any function $\omega = \omega(x)$, the jump of ω is defined as,

$$
[\![\omega]\!]_{ij} := \omega_i \boldsymbol{n}_{ij} + \omega_j \boldsymbol{n}_{ji} = \left(\omega_i - \omega_j\right)\boldsymbol{n}_{ij} \qquad \text{Eq. 19}
$$

and the weighted average of ω as:

$$
\{\omega\}_{ij} = \omega_i w_{ij} + \omega_j(1 - w_{ij}). \qquad \text{Eq. 20}
$$

Taking $w_{ij} = 0.5$ leads to the simple arithmetic averaging. Based on Ern et al. (2008), to better take the heterogeneity of the porous medium into account we here take:

$$
w_{ij}^n = \frac{\alpha_j^n}{\alpha_i^n + \alpha_j^n} \qquad \text{Eq. 21}
$$

where $\alpha^n = k\lambda_T^n.\ \gamma_{ij}^n$ is the harmonic average of α^n values in the two neighbouring cells for the interior faces $\sigma_{ij} \in \varepsilon_\Omega$ (Jamei and Ghafouri, 2016):

$$
\gamma_{ij}^n = \frac{2 \times \alpha_i^n \alpha_j^n}{\alpha_i^n + \alpha_j^n} \qquad \text{Eq. 22}
$$

This value reduces to α_i^n in Dirichlet boundaries. To reconstruct conservative fluxes from the DG solution we compute:

$$
v_{ij}^{n+1} = \begin{cases} \displaystyle\int_{\sigma_{ij}} \left\{\left(k_i\lambda_{T_i}^n\right)\boldsymbol{z}_i^{n+1}\right\}.\boldsymbol{n}_{ij} + \frac{\eta\gamma_{ij}^n}{h_{ij}}[\![p_i^{n+1}]\!].\boldsymbol{n}_{ij}\,, & on\ \varepsilon_\Omega, \\ \displaystyle\int_{\sigma_{ij}} \left(k_i\lambda_{T_i}^n\right)\boldsymbol{z}_i^{n+1}.\boldsymbol{n}_{ij} + \frac{\eta\gamma_{ij}^n}{h_{ij}}\left(p_i^{n+1} - p_D\right), & on\ \varepsilon_D. \end{cases} \qquad \text{Eq. 23}
$$

which corresponds to Eq. 18 with the test function $\omega = 1$.

3.4 Fast front tracking technique

We have developed a fast front tracking technique (FFrT) to estimate the position of the saturation discontinuity without solving the transport equation in each cell of the domain. Considering a two-phase flow problem like a waterflood, we suppose that the saturation takes only two values corresponding to

the saturation ahead of the front (typically s_{w_i}) and behind the front (typically s_f), the saturation corresponding to the Buckley-Leverett shock front. The mobility ratio between both fluids corresponds to the mobility ratio at the front (Hagoort, 1974; King and Dunayevski, 1989; Noetinger et al., 2004; Spesivtsev and Teodorovich, 2007; Teodorovich et al., 2011). The idea is that the velocity of the front is mainly controlled by the interplay between the heterogeneity of absolute permeability and the mobility jump at the front, and not by the rarefaction wave behind the front that is continuously spreading during the time. This method is an extreme simplification of the initial problem to compute a fast estimation of the location of the water-oil interface based on some concepts from pore network modelling and Buckley Leverett equation. The FFrT method is an initial value problem, meaning that it computes the position of the interface from the given initial position of the front or the saturation discontinuity. According to the method of characteristics applied to the Buckley-Leverett equation, the velocity of the slice of the porous medium with a saturation s, $\mathbf{v}|_s$, is:

$$\boldsymbol{v}|_s = \frac{\boldsymbol{v}}{\phi}\frac{\partial f_w}{\partial s}\Big|_s \qquad \text{Eq. 24}$$

In other words, if at the point $\boldsymbol{x}_f$ and at time t_1 the saturation is equal to s_f, it is still equal to this value at the position $\boldsymbol{x}_f + \Delta t \frac{\boldsymbol{v}}{\phi}\frac{\partial f_w}{\partial s}\Big|_{s=s_f}$ and at time $t_1 + \Delta t$.

3.4.1 Formulation

We define ζ_F^n as the set of all faces σ_{ij} where the front crosses the segment $(\boldsymbol{x}_i, \boldsymbol{x}_j)$. $\boldsymbol{x}_i$ and $\boldsymbol{x}_j$ represent the cell centres of the cells i and j. $\boldsymbol{x}_j$ represents the downstream cell depending on the direction of the flow (see Figure 1). ζ_F^0 is initialized depending on the initial conditions of the transport problem. Now, consider that we are at time step n of the simulation. After solving the pressure equation to obtain new pressure and fluxes, using the DG scheme (Eq. 17 - Eq. 18), we advance the front, in the following detailed steps:

(1) The Welge tangent method is used to construct the saturation at the front, s_f, analytically (Welge, 1952):

$$\frac{\partial f_w}{\partial s}\Big|_{s=s_f} = \frac{f_w(s_f) - f_w(s_{w_i})}{s_f - s_{w_i}} \qquad \text{Eq. 25}$$

For the case of quadratic relative permeabilities, the equation above gives the saturation at the front as a function of the viscosity ratio, $M = \mu_o/\mu_w$, as follows:

$$s_f = 1/\sqrt{1+M} \qquad \text{Eq. 26}$$

(2) We compute the velocity at the front, $v_{f,i,j}^{n+1}$, using the discretized form of Eq. 24 and the total fluxes v_{ij}^{n+1}:

$$v_{f,i,j}^{n+1} = \frac{v_{ij}^{n+1}}{|\sigma_{ij}|\phi}\frac{\partial f_w}{\partial s}\Big|_{s_f} \qquad \text{Eq. 27}$$

(3) Considering that only the normal component of velocity accounts for the local velocity at the front, the discretized front is advanced according to the ordinary interface evolution equation:

$$\frac{\boldsymbol{x}_{f,i,j}^{n+1} - \boldsymbol{x}_{f,i,j}^{n}}{\delta t^{n+1}} = v_{f,i,j}^{n+1} \boldsymbol{n}_{ij} \qquad \text{Eq. 28}$$

δt^{n+1} denotes the sub-timestep for the update of the front position.

(4) We define the sub-timestep by posing a condition that measures the smallest time to reach the cell centre:

$$\delta t^{n+1} = \min_{\sigma_{ij} \in \zeta_F^n} \left(\frac{\left\| \boldsymbol{x}_j - \boldsymbol{x}_{f,i,j}^{n} \right\|}{v_{f,i,j}^{n+1}} \right) \qquad \text{Eq. 29}$$

$\boldsymbol{x}_{f,i,j}^{n}$ represents the current position of the front between two adjacent cells i and j (see Figure 1)

We repeat the steps (3) and 0 until the sum of all δt^{n+1} will be equal to the time step in the main scheme, Δt^{n+1}. Doing so, all the blocks where the front moves to are marked to remain at a higher resolution.

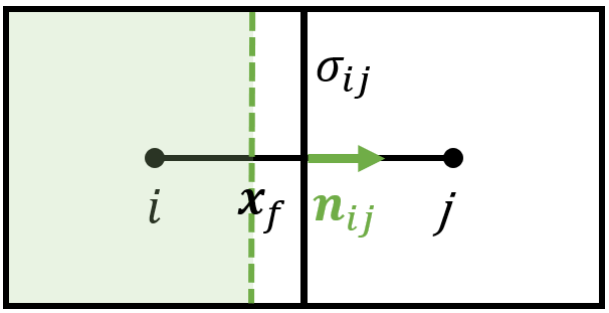

Figure 1 the two cells and the front position used to define the algorithm

3.4.2 Test case validation

To verify the proposed FFrT method, we consider two-dimensional water-flood problems, where oil is displaced by the water of the same or different viscosity. Both fluids are incompressible. The reservoir is initially filled with oil. Water is injected from the left boundary of the domain.

The Buckley Leverett problem:

We create a simple example to compare the proposed fast front tracking method with the Buckley Leverett (BL) solution. We choose a $10 \times 2\ m^2$ domain, discretised by a 200×50 Cartesian grid. The permeability and porosity are spatially homogeneous and equal to 0.01 Darcy and 1.0, respectively. Water is injected from the left boundary with a constant rate of $10^{-6}\ m^3/s$ ($4.3e-3$ PV/day). The viscosity of oil is set to $10\ cp$. The viscosity of water varies between three different values of $1, 3.33, \text{and } 10\ cp$, in different cases. Figure 2 shows some comparisons of the FFrT method with the BL solution for different viscosity ratio cases and at different time steps.

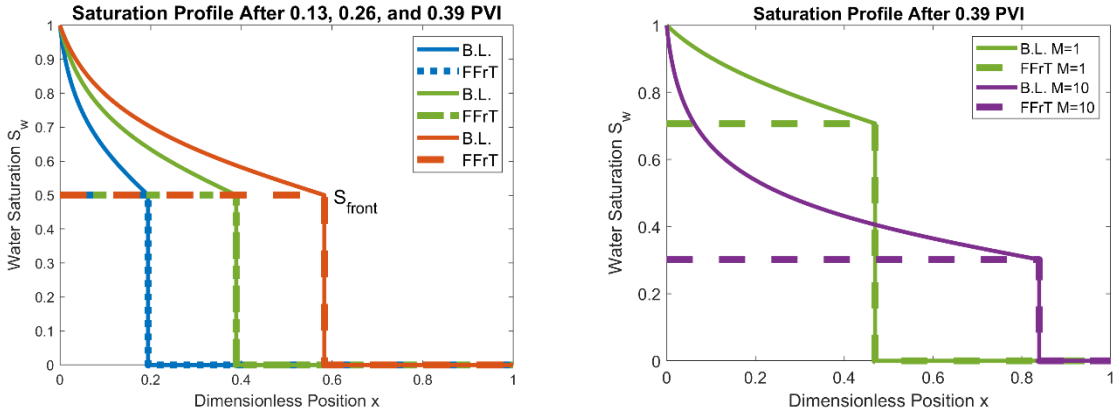

Figure 2 The comparison of the proposed FFrT method with the analytical solution of the BL equation for (a) a viscosity ratio of $M = \mu_o/\mu_w = 3$, at three different times and (b) for two different viscosity ratio M=1 & 10, after 0.39 pore volume injected.

Random generated isotropic medium:

To increase the complexity of the validation cases, we test the method with a smoothly heterogeneous random permeability field generated with a lognormal distribution, a correlation length of 0.1, and a Dykstra-Parsons coefficient of 0.2, shown in Figure 3. We set Dirichlet conditions on the left and right boundaries, and a no-flow condition on the top and bottom boundaries. We consider the previously described two-phase flow problem. We set the viscosity of oil to 10 cp and consider different viscosity ratios. The original computational grid contains 100×100 cells. Figure 4 shows water saturation contour maps computed using a standard FV IMPES (implicit pressure - explicit saturation) scheme and the FFrT method for four viscosity ratios. The analytical saturation of the front is also shown for each case of the viscosity ratio M, computed using Eq. 26. In the case of a unit viscosity ratio with a relatively sharp front, the prediction of the FFrT method is in good accordance with the saturation profile computed using the standard FV scheme. When the viscosity ratio M increases and the front becomes more distorted, a small difference between the predicted front position and the FV solution can be observed. Due to numerical errors inherent to both methods and lack of an exact solution it may be difficult to interpret the difference. It is worth noting that the proposed fast front tracking method cannot predict the rarefaction wave behind the front and the numerical diffusion of the front. The essential fact is that the frontal zone is captured correctly. This allows to set-up correctly the adaptive coarsening strategy with the FFrT method as a criterion, which is our main goal in the proposed workflow.

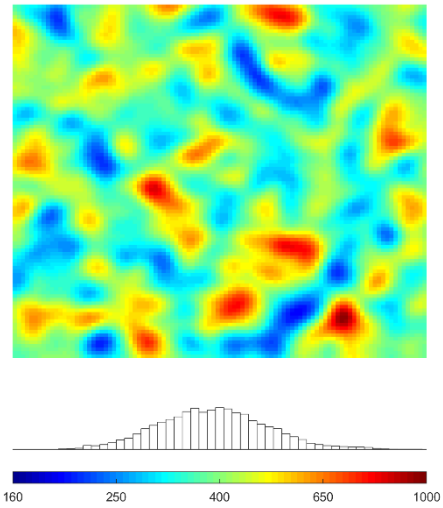

Figure 3 Isotropic randomly generated permeability model with a dimensionless correlation length of 0.1 and Dikstra-Parson coefficient of 0.2 in the logarithmic scale

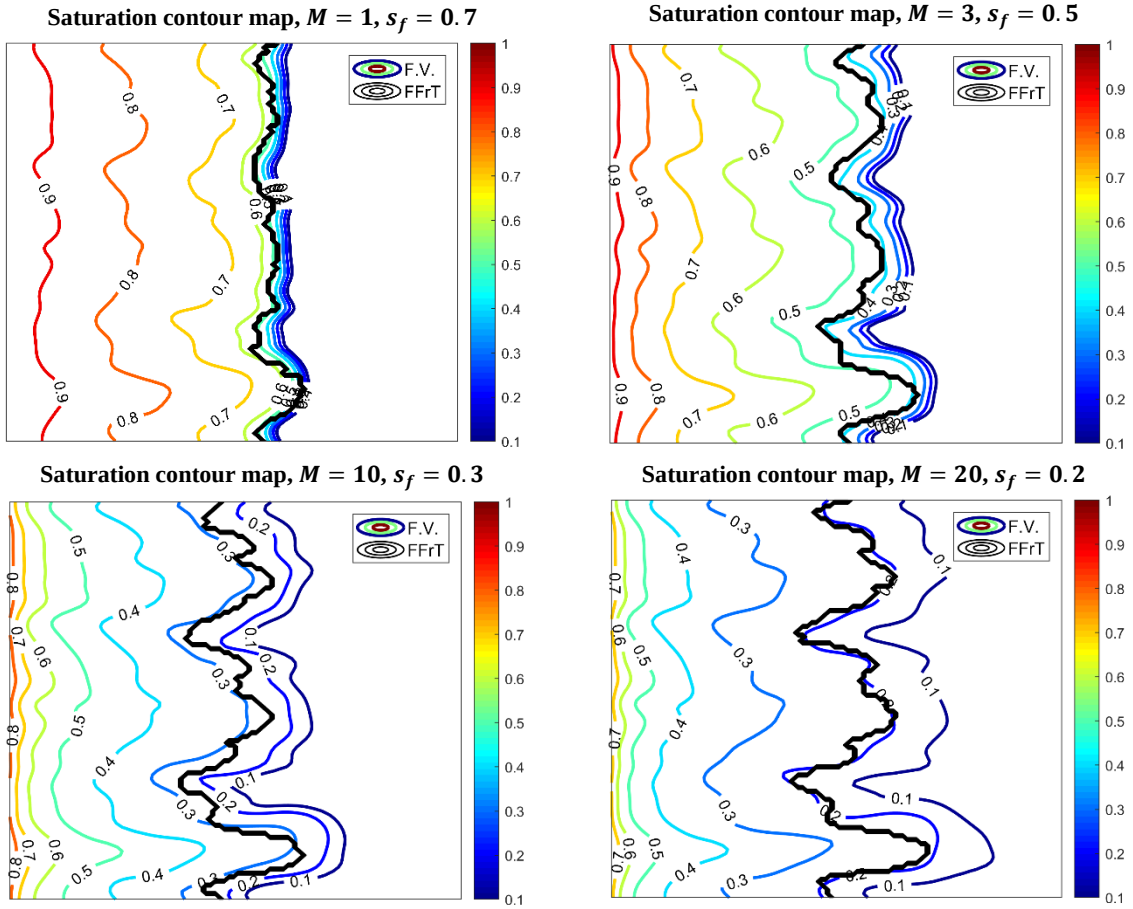

Figure 4 Water saturation contour maps for the randomly generated permeability domain shown in the previous figure with different cases of viscosity ratio, computed by the proposed FFrT method and a standard FV scheme.

SPE 10 benchmark test:

We consider a two-dimensional Cartesian model with permeability values taken from the second SPE10 benchmark test (Christie and Blunt, 2001). This model contains $60 \times 220 \times 85$ cells, in which the top 35 layers represent Tarbert formation and the bottom 50 layers represent Upper Ness formation. We consider the same immiscible two-phase flow (water-oil) problem with the same initial and boundary

conditions as in the previous example, on both the original fine and coarsened grids. We generate the coarse grid via a uniform agglomeration of the base fine grid, with an agglomeration ratio of 10. We use a flow-based upscaling method to compute the upscaled permeabilities (Chen et al., 2003), where a set of representative boundary conditions are imposed at the coarse grid blocks to solve the flow equation and use the fine-scale pressure and fluxes to compute the upscaled permeabilities. The fine-scale and upscaled permeability maps for the layers 22 and 70 of the SPE10 dataset are shown in Figure 5. In Figure 6 we compare the FFrT method with a standard finite volume scheme at two resolutions, for a waterflood problem with a viscosity ratio $M = 10$ in layer 22 of SPE 10 model. At the coarse scale, the results of FFrT method are very close to the FV solution of the same resolution. In the fine-scale simulation, the FFrT method predicts the flow patterns very well, and the main difference with the fine-scale simulation is close to the right boundary, where the front becomes diffusive. For a more detailed comparison, the superimposed contour maps for the original resolution case are shown in Figure 7. This figure shows that the predicted front position is very close to the saturation contour line of 0.3, computed using the FV scheme on the original grid.

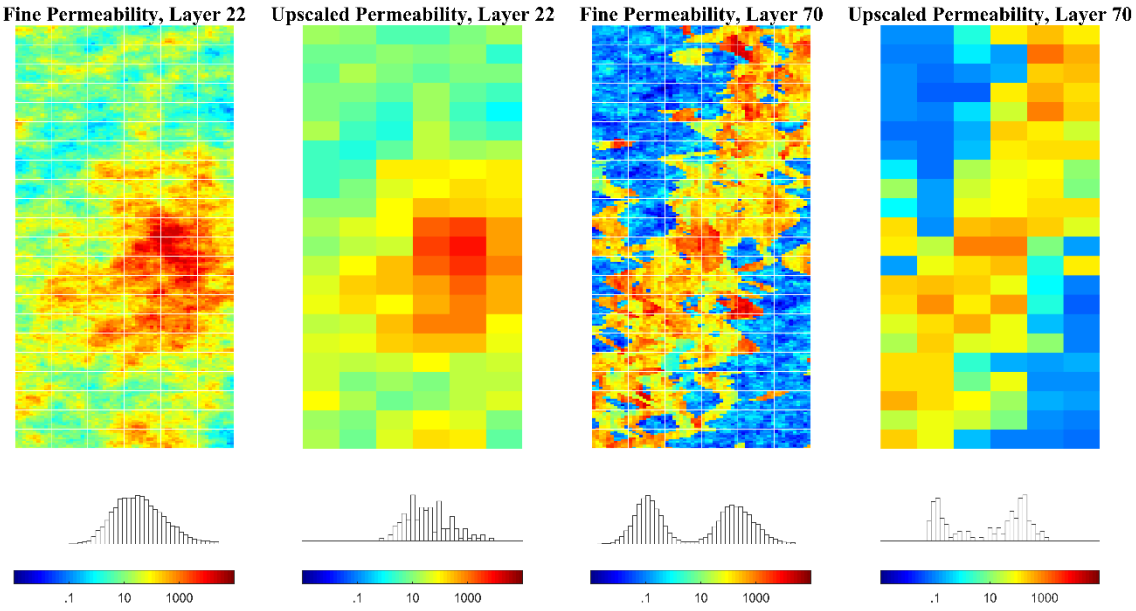

Figure 5 Permeability maps of the layers 22 and 70 of SPE10 model in the logarithmic scale, before and after upscaling

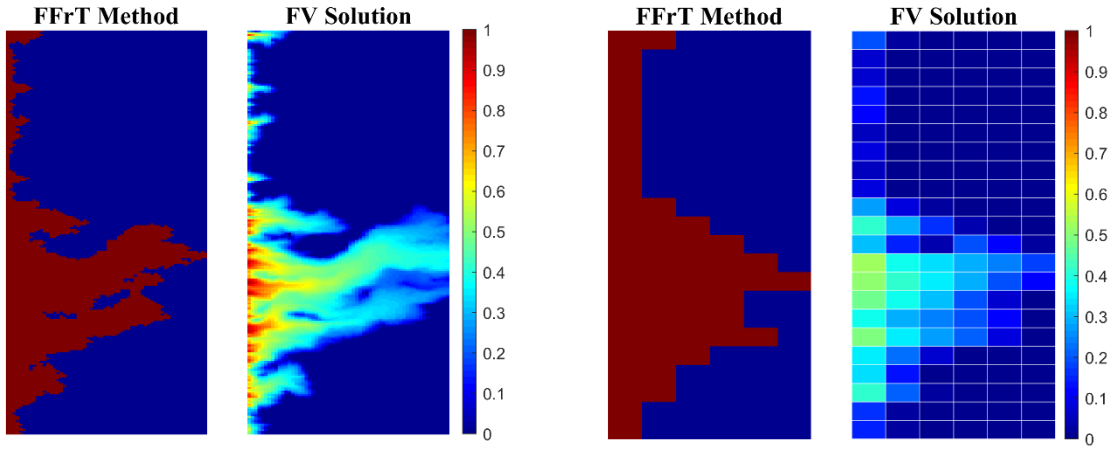

Figure 6 Water saturation maps for layer 22 of SPE 10 model for a waterflood problem with the viscosity ratio of 10 at the original and a coarsened resolution, computed by the FFrT and FV methods.

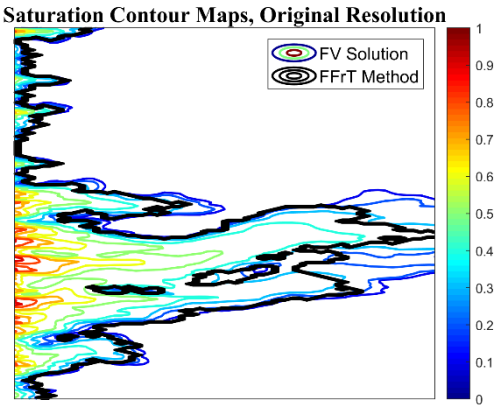

Figure 7 Water saturation contour maps for layer 22 of SPE 10 model, for the same time step as the previous figure, at the original fine resolution.

4 The solution flow chart

We now detail the complete solution procedure at each time step using the previous schemes and the FFrT technique:

(1) The pressure equation is solved using the DG scheme with a linear approximation on the base coarse grid over the whole domain.

(2) DG conservative fluxes are reconstructed and then the front is moved using the FFrT method. This step includes solving Eq. 28 in some parts of the domain. The position of the front is then used to (1) partition the domain into single- and multiphase-phase flow regions and (2) use a higher resolution grid, equal to the resolution of the original fine grid or an intermediate resolution, where the front moves. One immediate advantage of domain partitioning is to solve the saturation equation only in the multi-phase flow region. As a result, no multiphase upscaling method is needed. We use the dynamic coarsening approach of Hauge et al. (2012) to use a higher-resolution grid where the criterion is met.

(3) Flow and transport problems are solved in the multiphase flow part of the domain, on an adaptively coarsened grid generated at the previous step. Depending on the type of faces, boundary or interior ones between single-phase and two-phase flow regions, the boundary pressure or the DG conservative fluxes are set as boundary conditions. These boundary conditions are used to solve the pressure and transport problems using the FV method. Except for the DG and the FFrT, our methodology use tools for the upscaling, the dynamic mesh coarsening, and the FV resolutions that are available in the MATLAB Reservoir Simulation Toolbox, MRST[2] (Lie, 2019; Lie et al., 2012). A flowchart of the proposed approach is illustrated in Figure 8.

[2] https://www.sintef.no/projectweb/mrst/

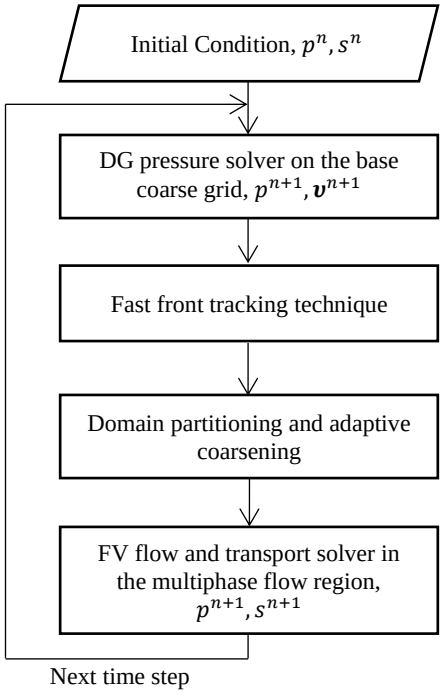

Figure 8 The flow chart of the proposed sequential approach for each time step

4.1 Complexity analysis

We use the number of unknowns solved at each step as the main indicator of the complexity of the solution approach so that this analysis does not depend on the actual implementation of the method. In the following, we detail the computational cost of each step separately.

(1) DG pressure solver on the base coarse grid: The number of unknowns at this step is equal to the number of coarse grid blocks times the number of local degrees of freedom which is equal to:

$$N = (P+1)^2 \qquad \text{Eq. 30}$$

where P is the polynomial degree.

(2) The FFrT method: In this step, Eq. 28, is solved in parts of the domain where the front is present, and the number of unknowns here depends on the shape of the front. Thanks to these two important features, being local to cells where the front is present, and the explicitness of the equation to be solved, this step is computationally very fast.

(3) Adaptive coarsening: In the agglomeration-based coarsening approaches, a coarse grid is generated from the agglomeration of the fine grid using a partition vector to relate coarse blocks to their underlying fine cells. Thanks to this preserved one-to-one mapping between fine and coarse grids, adding or removing local resolution is simple to carry out. Even if the cost of the grid adaptations is difficult to quantify precisely, in test cases we performed, this step was less than about five per cent of our overall computational time. It is also worth noting that this dynamic coarsening reduces the number of unknowns in the computationally demanding transport solver.

(4) FV pressure and transport solver in the refined areas: The number of unknowns in this step is twice the number of cells in the two-phase flow region.

As an illustrative example, we test the method with the random permeability field of Figure 3. Water and oil viscosities are equal to 1.0 and 0.2 cp, respectively. The reservoir is initially filled with oil. A coarse grid is generated by uniform agglomeration of the original grid with a coarsening ratio of 10. This simple example with sharp and smooth fronts shows how the proposed approach works. Figure 9 shows the resulting saturation maps along with the fine solution taken as reference. The second plot, from left, shows a pseudo saturation map that indicates the presence or absence of water given by the FFrT method. The third plot shows the results of the domain partitioning scheme, where the saturation equation is solved using the FV method only in the identified two-phase region with a high-resolution grid. The green lines show the boundaries of the two-phase region. This domain is only defined from its west and east boundaries. The north and south boundaries coincide with the main boundaries of the reservoir. The east boundary is determined thanks to the pseudo saturation map. Since this criterion cannot be used to determine the west boundary of the domain, the saturations calculated from the previous time step are used instead. The last plot in this figure shows the results obtained with our procedure, where both domain partitioning and dynamic nonuniform coarsening are used. Figure 10 shows the ratio of the total number of global degrees of freedom in the proposed approach compared to the reference solution for this example.

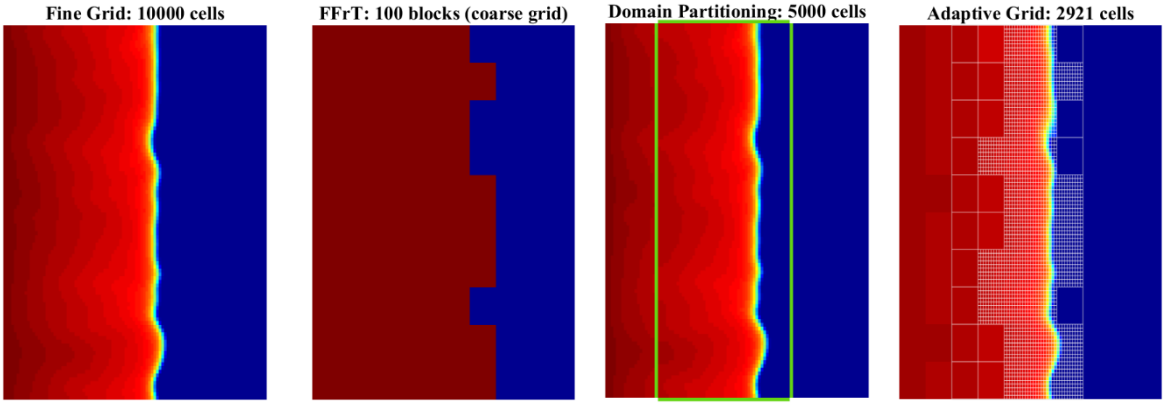

Figure 9 From left to right: the water saturation map on the base fine grid taken as the reference solution, the pseudo-saturation map on the coarse mesh based on FFrT method, the water saturation map for the domain partitioning scheme (without adaptive coarsening), and the results obtained with the proposed approach using domain partitioning and adaptive coarsening. The green line indicates the two-phase partition of the domain. The number of grid cells is shown above each plot.

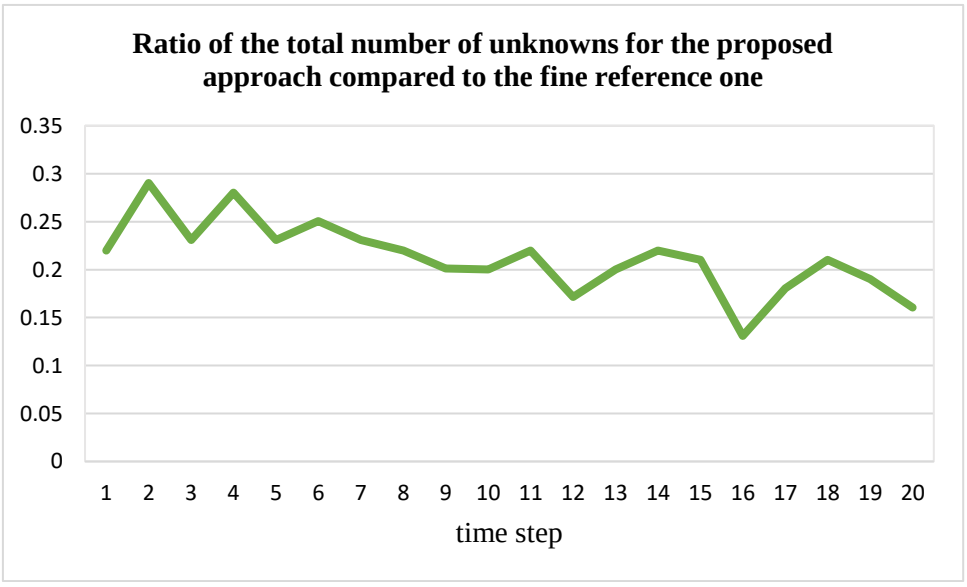

Figure 10 The ratio of the total number of unknowns to be solved at each time step in the proposed solution approach compared to the fine reference solution.

5 Numerical Examples

In the following examples, we test the approach in two-dimensional waterflood problems with favourable and unfavourable viscosity ratios. The initial and boundary conditions remain the same as in the previous examples. In the first two examples, the identified coarse blocks are replaced with their underlying fine grid cells. In the third example, we present cases where the resolution of the identified coarse blocks are increased to an intermediate level.

5.1 Example 1: Favourable displacement

We test the proposed solution strategy in a favourable displacement process in a two-dimensional Cartesian model with permeability values taken from layer 70 of the second SPE10 benchmark test. Figure 11 shows the water saturation maps at three different time steps in this channelized reservoir. The viscosity of water is 1.0 cp and the viscosity of oil is 0.2 cp. We can see that our proposed approach captures the channelized flow detail which is challenging to get when a low-resolution grid is used over the whole domain. In this figure, we also compare the proposed FFrT technique with a classic criterion, where the saturation equation is solved on a coarse grid and the saturation change from the previous time step is used to locally increase the mesh resolution in the blocks where this change exceeds a defined tolerance. The FV solution on the original fine grid is also shown as a reference. To evaluate the accuracy of DG conservative fluxes, the results of the finite volume transport solution using DG computed total fluxes on the coarse grid are computed. We can see in this example that FFrT method gives a better indication of where to add a higher spatial resolution. The proposed FFrT method solves an explicit equation on some parts of the domain, while the saturation gradient criterion needs the solution of the transport equation over the whole domain. To evaluate the accuracy of the proposed approach, we use the L^1 relative error norm to compare the proposed solution strategy with the reference fine solution, computed using the equation below:

$$err_h = \frac{\left\| s_h - s_{ref} \right\|_{L^1(\Omega)}}{\left\| s_{ref} \right\|_{L^1(\Omega)}} \qquad \text{Eq. 31}$$

where s_{ref} is the reference solution where finite volume is used for solving both equations on the original fine grid, and s_h represent the saturation in the chosen solution strategy. A comparison of the errors and water cuts obtained with different schemes are shown in Figure 12. The proposed scheme gives satisfactory results in terms of error, water breakthrough time, and the water cut. In these plots, the results of the finite volume solution on the coarse grid are shown as well. In terms of error, the DG conservative fluxes give results close to the finite volume coarse resolution. Figure 13 shows the ratio of the total number of degrees of freedom for each time step for the proposed approach compared to the base fine solution. The number of unknowns and subsequently the computational efficiency of the approach depends on the extension of the multiphase flow area over the domain. It also depends on the spatial resolution of the refined subdomains. In this example, water breakthrough happens early during the simulation and the multiphase subdomains are replaced with their underlying fine grid cells.

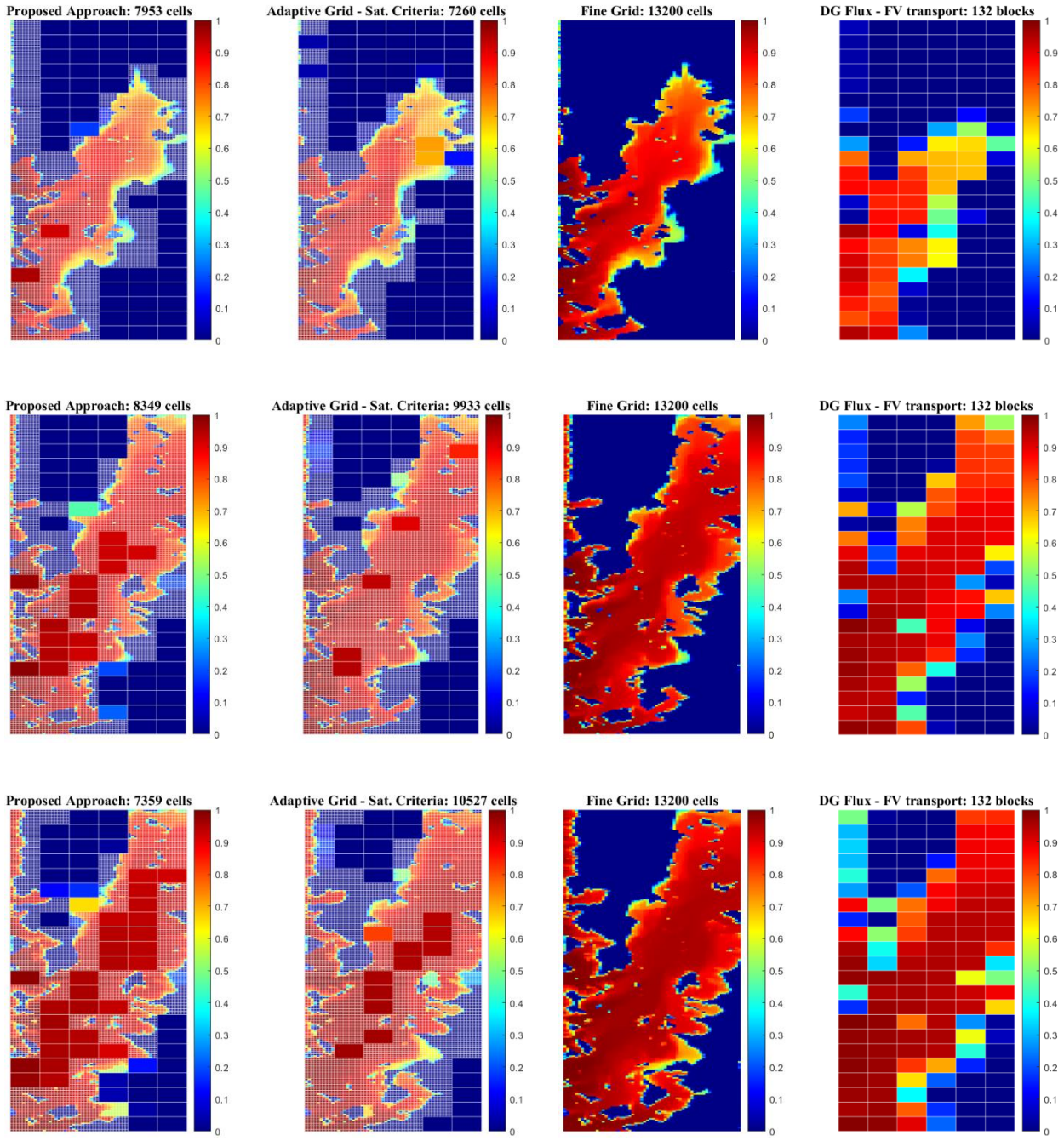

Figure 11 Saturation maps for the layer 70 of the SPE10 model computed by the proposed approach, the adaptive approach with saturation gradient criteria, FV on the base fine grid, and DG(flux)-FV(saturation) schemes, at three different time steps.

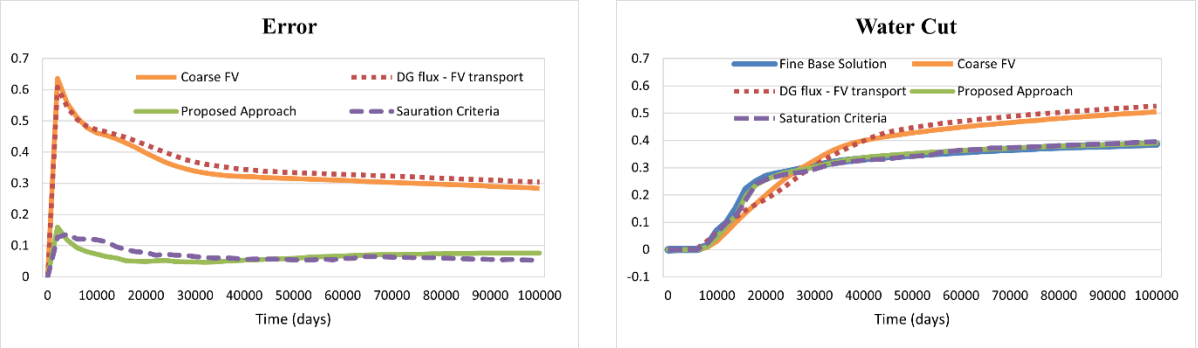

Figure 12 Errors and water cut as a function of time for the layer 70 of the SPE10 model in a favourable displacement process

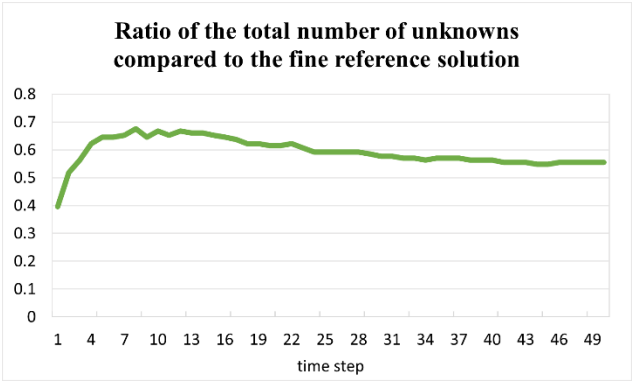

Figure 13 The ratio of the total number of unknowns for each time step in the proposed approach compared to the base fine solution

5.2 Example 2: Unfavourable displacement

To test the proposed solution strategy in unfavourable viscosity ratios, we set the viscosities of water and oil to 0.5 and 5 *cp*, respectively, to get an unstable viscous flow at the front. All other conditions remain the same as in the previous case. Figure 14 shows the water saturation maps at three different time steps for the same layer. Our proposed approach successfully captures the diffusive flow pattern in the channel. Water saturation gradient works slightly better than the FFrT in the early time steps but tends to decline after the water breakthrough time. Figure 15 shows the errors and water cuts for different schemes. We notice that in this case, the coarse DG conservative fluxes give slightly better results than the coarse FV fluxes, in terms of the water cuts. The dynamic coarsening approaches with FFrT method and the classical criterion of saturation gradient give similar results in terms of relative error and water cut. However, the FFrT method is much faster than any transport solver. This figure also shows the relatively large errors in coarse-scale solutions. Figure 16 shows the total number of global degrees of freedom for the proposed approach relative to the reference fine solution. The proposed approach has an accuracy close to the reference solution while decreasing the number of global degrees of freedom.

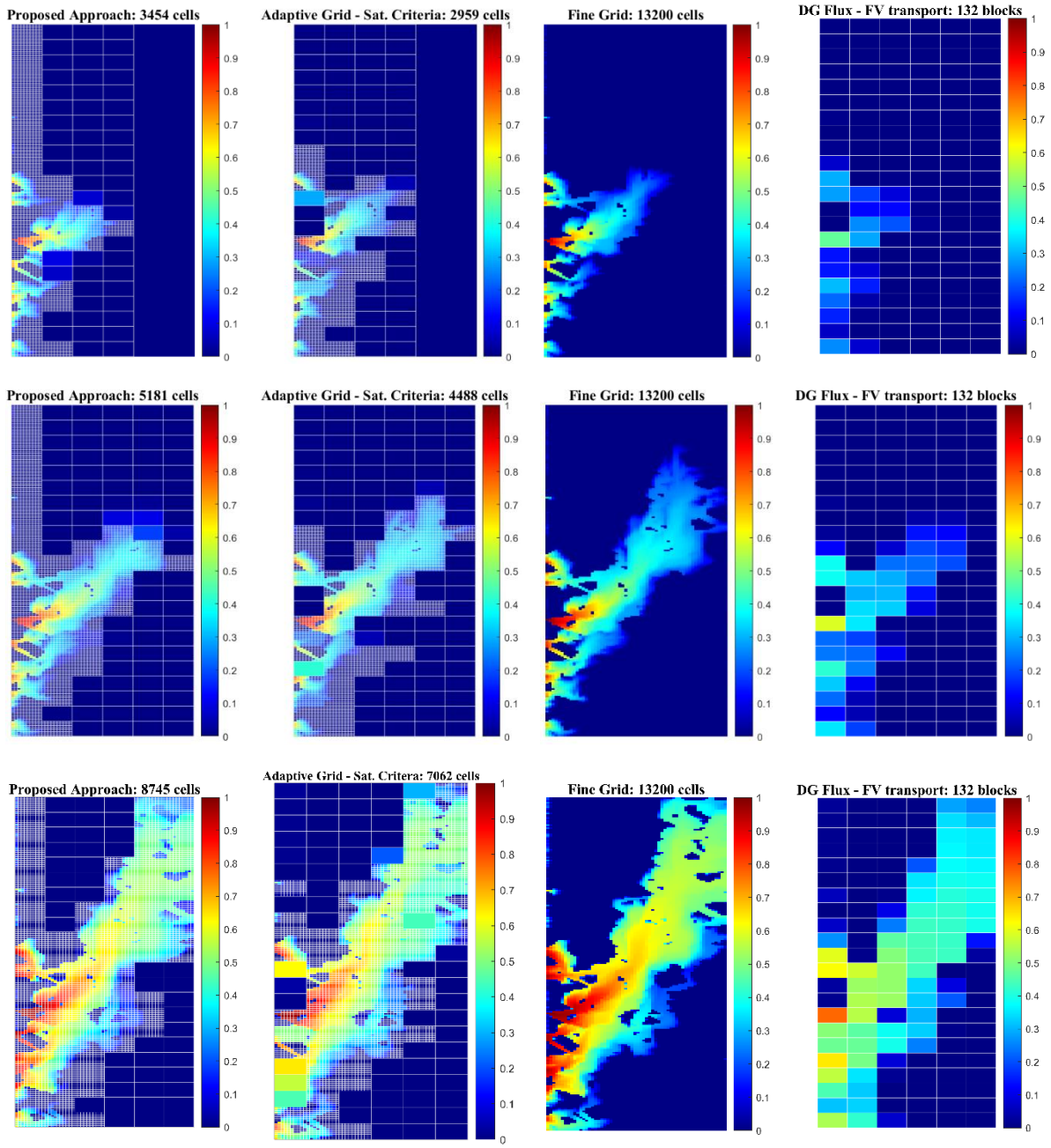

413 Figure 14 Water saturation maps for the layer 70 of the SPE10 model, at three different time steps
414 before (first row), at (second row), and after (third row) the water breakthrough for an unfavourable
415 displacement case.

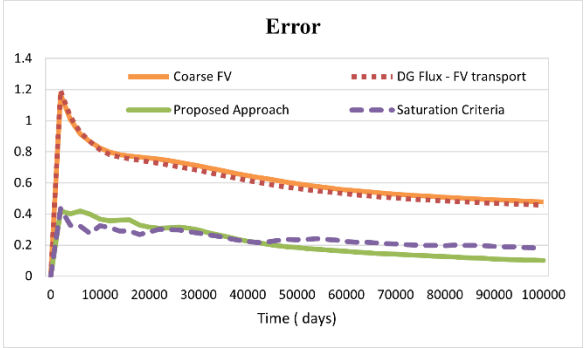

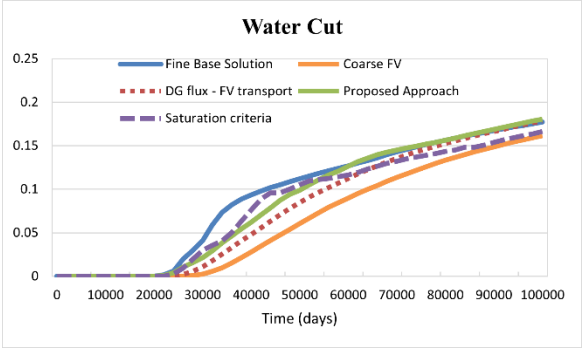

Figure 15 Errors and water cuts as a function of time for the layer 70 of the SPE10 model with an unfavourable viscosity ratio.

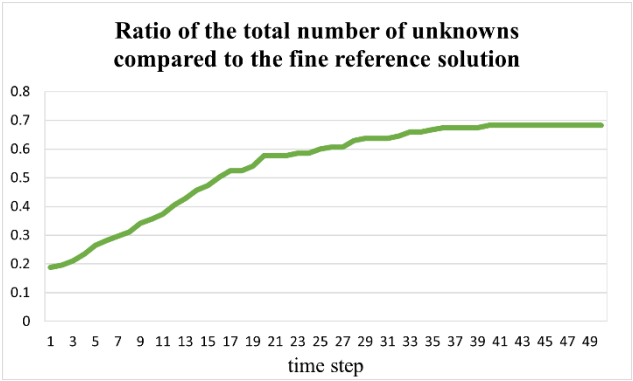

Figure 16 The ratio of the total number of unknowns for each time step in the proposed approach compared to the base fine solution for the unfavourable displacement in layer 70 of SPE10 benchmark test

5.3 Example 3: Intermediate resolution

In the previous examples, we replaced the coarse blocks with their original fine resolution grid cells in the adaptive coarsening step. But we can also increase the spatial resolution in the indicated coarse grid blocks to any intermediate resolution, to decrease the number of degrees of freedom and ultimately improve the computational efficiency. This is especially more efficient in displacements with sharp saturation fronts. In Figure 17 you can see the results of the approach using an intermediate spatial resolution, where the identified coarse blocks are replaced with a finer resolution of ratio 2 relative to the original resolution. Here the permeability field is taken from layer 22 of the SPE10 second model and viscosities of water and oil are set to 1.0 and 0.2 cp, respectively. The errors and water cuts are represented in Figure 18.

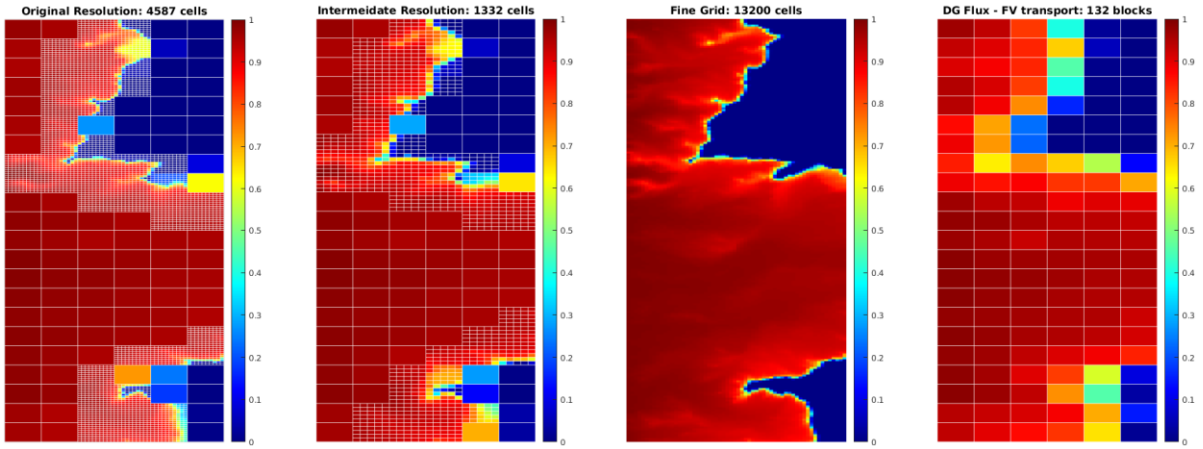

Figure 17 Saturation maps for layer 22 of the SPE10 with a favourable viscosity ratio, for two different fine resolutions.

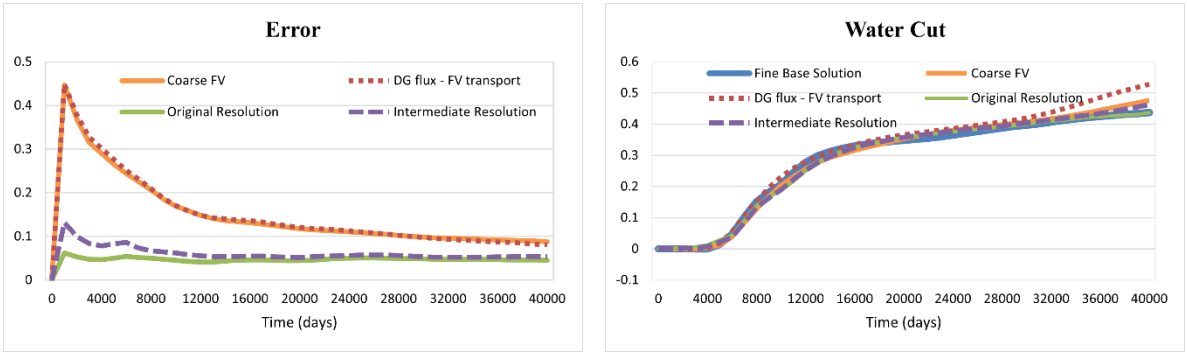

Figure 18 Errors and water cuts as a function of time for the layer 22 of the SPE10 model and two different intermediate resolutions.

We revisit the examples 5.1 and 5.2 and we increase the resolution of identified coarse blocks to different intermediate levels with agglomeration ratios of 2 and 4 relative to the base fine grid. Figure 19 shows the error, the water cut, and the total number of unknowns for both examples. In this figure, the original resolution represents the solution where the coarse blocks are replaced with their original fine cells. This figure shows that replacing the coarse blocks with an intermediate resolution of the agglomeration ratio 2 gives suitable accuracy while decreasing the total degrees of freedom to a great extent.

Example 1: Favourable displacement

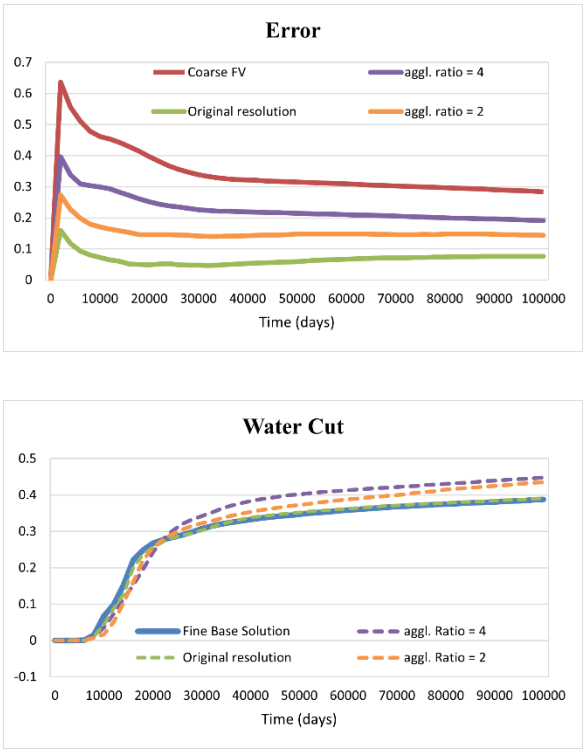

Example 2: Unfavourable displacement

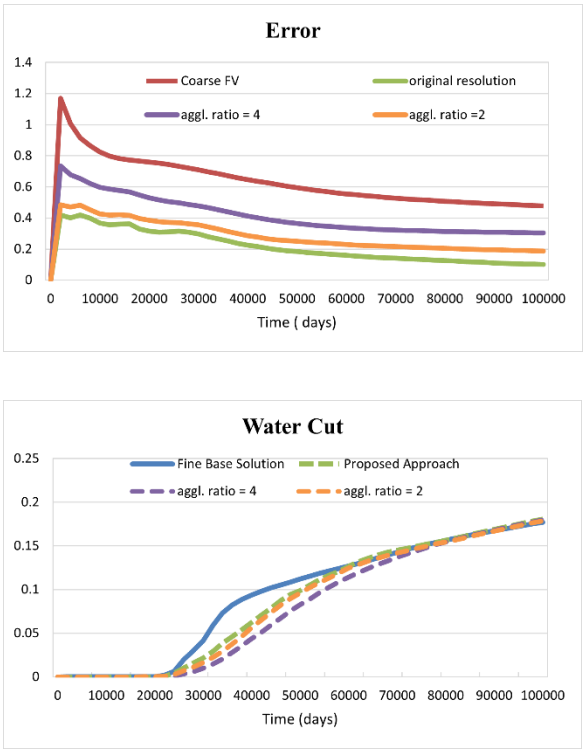

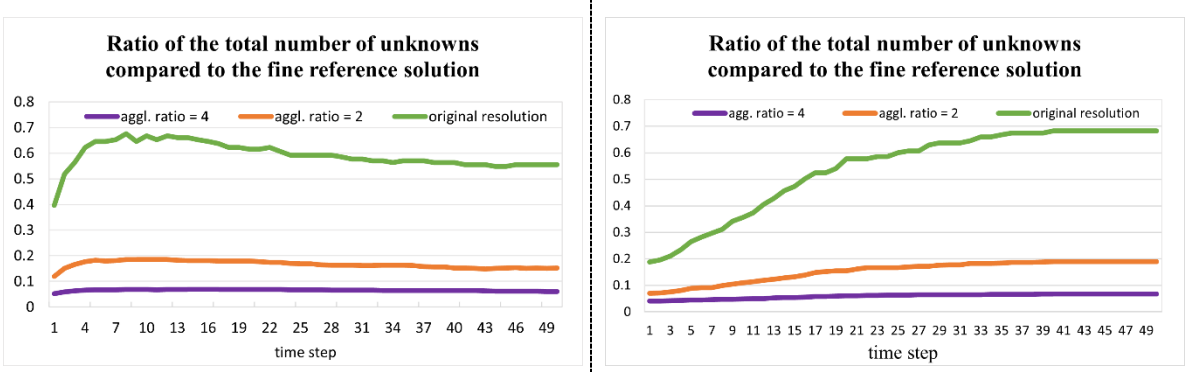

Figure 19 The errors, the water cuts, and the ratio of the total number of unknowns compared to the fine reference solution for the previous examples with different intermediate resolution level.

6 Conclusions

In this paper, an original method combining dynamic non-uniform coarsening and a discontinuous Galerkin method was developed. The goal is to improve the efficiency of multiphase flows simulations in heterogeneous porous media without losing accuracy. The proposed fast front tracking method appears as being a promising method to combine different resolution strategies focusing on different flow areas. This method can be used on a coarse scale to identify the two-phase flow region with satisfying accuracy and a small computational cost of solving an explicit equation in some parts of the domain. This information can thus be used as input to dynamic mesh coarsening and adaptive use of DG and FV solvers for the pressure equation. This method has proved to be a powerful tool to predict the position of the front. Near the front, in the two-phase region, we have shown that a high-resolution grid used along with a finite volume discretization leads to stable solutions with improved accuracy. Far from the front, the DG method, used on a lower resolution grid, increases the accuracy of the total velocity.

The efficiency of the approach depends on the overall spreading of the multiphase region, and the level of resolution in the adaptive coarsening. We have shown that the resolution level can be adjusted depending on the required order of accuracy, the available computational cost, and the complexity of the problem.

However, the proposed solution strategy can be extended to a more general framework. The fast front tracking method can be improved to handle more complex flows like radial ones around wells in 3D domains. Other approaches could also be followed. For example, working at a coarse-scale using classical single-phase upscaling, coupled with up-scaled two-phase flow equations with an effective fractional flow function (Artus et al., 2004; Fayers et al., 1992; Sorbie et al., 1995) and a macrodispersion term modelling the subgrid disorder. The effective fractional flow accounts for the average local pressure saturation coupling. This could help to get a fast estimation of the front location and its typical thickness at the coarse scale directly. If necessary, a mesh refinement will then be set up in that area depending on a posteriori criterion quantifying the overall accuracy of the calculation (Gratien et al., 2016).

References

Abdul Hamid, S.A., Muggeridge, A.H., 2018. Analytical solution of polymer slug injection with viscous fingering. Comput Geosci 22 (3), 711–723. https://doi.org/10.1007/s10596-018-9721-0.

Artus, V., Nœtinger, B., Ricard, L., 2004. Dynamics of the water–oil front for two-phase, immiscible flow in heterogeneous porous media. 1–stratified media. Transport in porous media 56 (3), 283–303.

Ashjari, M.A., Firoozabadi, B., Mahani, H., Khoozan, D., 2007. Vorticity-based coarse grid generation for upscaling two-phase displacements in porous media. Journal of Petroleum Science and Engineering 59 (3-4), 271–288. https://doi.org/10.1016/j.petrol.2007.04.006.

Barker, J.W., Dupouy, P., 1999. An analysis of dynamic pseudo-relative permeability methods for oil-water flows. Petroleum Geoscience 5 (4), 385–394.

Barker, J.W., Thibeau, S., 1997. A critical review of the use of pseudorelative permeabilities for upscaling. SPE reservoir engineering 12 (2), 138–143.

Bastian, P., 2014. A fully-coupled discontinuous Galerkin method for two-phase flow in porous media with discontinuous capillary pressure. Computational Geosciences 18 (5), 779–796. https://doi.org/10.1007/s10596-014-9426-y.

Bastian, P., Riviere, B., 2004. Discontinuous Galerkin methods for two-phase flow in porous media. University of Heidelberg Technical Report 28, 2004.

Cappanera, L., Riviere, B., 2019. Discontinuous Galerkin method for solving the black-oil problem in porous media. Numer. Methods Partial Differential Eq. 35 (2), 761–789. https://doi.org/10.1002/num.22324.

Chen, Y., Durlofsky, L.J., Gerritsen, M., Wen, X.H., 2003. A coupled local–global upscaling approach for simulating flow in highly heterogeneous formations. Advances in water resources 26 (10), 1041–1060. https://doi.org/10.1016/s0309-1708(03)00101-5.

Christie, M.A., 1996. Upscaling for reservoir simulation. Journal of Petroleum Technology 48 (11), 1,004-1,010.

Christie, M.A., Blunt, M.J., 2001. Tenth SPE Comparative Solution Project: A comparison of upscaling techniques, in: . SPE Reservoir Simulation Symposium. Society of Petroleum Engineers.

Colecchio, I., Boschan, A., Otero, A.D., Noetinger, B., 2020. On the multiscale characterization of effective hydraulic conductivity in random heterogeneous media: A historical survey and some new perspectives. Advances in water resources 140, 103594. https://doi.org/10.1016/j.advwatres.2020.103594.

Correia, M.G., Maschio, C., Schiozer, D.J., 2018. Flow simulation using local grid refinements to model laminated reservoirs. Oil & Gas Science and Technology - Rev. IFP Energies nouvelles 73, 5. https://doi.org/10.2516/ogst/2017043.

Darban, A., Ghaedi, M., Qajar, J., 2020. Analysis of the impacts of relative permeability and mobility ratio on heterogeneity loss error during upscaling of geological models. Oil Gas Sci. Technol. – Rev. IFP Energies nouvelles 75, 53. https://doi.org/10.2516/ogst/2020049.

Darman, N.H., Pickup, G.E., Sorbie, K.S., 2002. A comparison of two-phase dynamic upscaling methods based on fluid potentials. Computational Geosciences 6 (1), 5–27.

Datta-Gupta, A., King, M.J., 2007. Streamline simulation: Theory and practice. Society of Petroleum Engineers Richardson.

Di Pietro, D.A., Ern, A., 2011. Mathematical aspects of discontinuous Galerkin methods. Springer Science & Business Media.

Durlofsky, L.J., 1991. Numerical calculation of equivalent grid block permeability tensors for heterogeneous porous media. Water Resources Research 27 (5), 699–708.

Durlofsky, L.J., Jones, R.C., Milliken, W.J., 1997. A nonuniform coarsening approach for the scale-up of displacement processes in heterogeneous porous media. Advances in water resources 20 (5-6), 335–347.

Ern, A., Mozolevski, I., Schuh, L., 2010. Discontinuous Galerkin approximation of two-phase flows in heterogeneous porous media with discontinuous capillary pressures. Computer methods in applied mechanics and engineering 199 (23-24), 1491–1501.

Ern, A., Stephansen, A.F., Zunino, P., 2008. A discontinuous Galerkin method with weighted averages for advection-diffusion equations with locally small and anisotropic diffusivity. IMA Journal of Numerical Analysis 29 (2), 235–256. https://doi.org/10.1093/imanum/drm050.

Fabien, M.S., Knepley, M., Riviere, B., 2020. A high order hybridizable discontinuous Galerkin method for incompressible miscible displacement in heterogeneous media. Results in Applied Mathematics 8, 100089. https://doi.org/10.1016/j.rinam.2019.100089.

Farmer, C.L., 2002. Upscaling: A review. International Journal for Numerical Methods in Fluids 40 (1-2), 63–78.

Fayers, F.J., Blunt, M.J., Christie, M.A., 1992. Comparisons of empirical viscous-fngering models and their calibration for heterogeneous problems. SPE reservoir engineering 7 (02), 195–203. https://doi.org/10.2118/22184-PA.

Frank, F., Reuter, B., Aizinger, V., Knabner, P., 2015. FESTUNG: A MATLAB/GNU Octave toolbox for the discontinuous Galerkin method, Part I: Diffusion operator. Computers & Mathematics with Applications 70 (1), 11–46.

Ganjeh-Ghazvini, M., 2019. The impact of viscosity contrast on the error of heterogeneity loss in upscaling of geological models. Journal of Petroleum Science and Engineering 173, 681–689. https://doi.org/10.1016/j.petrol.2018.10.061.

Gratien, J.-M., Ricois, O., Yousef, S., 2016. Reservoir Simulator Runtime Enhancement Based on a Posteriori Error Estimation Techniques. Oil & Gas Science and Technology - Rev. IFP Energies nouvelles 71 (5), 59. https://doi.org/10.2516/ogst/2016009.

Hagoort, J., 1974. Displacement stability of water drives in water-wet connate-water-bearing reservoirs. Society of Petroleum Engineers Journal 14 (01), 63–74. https://doi.org/10.2118/4268-PA.

Han, D.K., Han, D.L., Yan, C.Z., Peng, L.T., 1987. A more flexible approach of dynamic local grid refinement for reservoir modeling, in: SPE Symposium on Reservoir Simulation. Society of Petroleum Engineers.

Hauge, V.L., Lie, K.-A., Natvig, J.R., 2012. Flow-based coarsening for multiscale simulation of transport in porous media. Computational Geosciences 16 (2), 391–408.

Jamei, M., Ghafouri, H., 2016. An efficient discontinuous Galerkin method for two-phase flow modeling by conservative velocity projection. Int Jnl of Num Meth for HFF 26 (1), 63–84. https://doi.org/10.1108/HFF-08-2014-0247.

Jaust, A., Reuter, B., Aizinger, V., Schütz, J., Knabner, P., 2018. FESTUNG: A MATLAB/GNU Octave toolbox for the discontinuous Galerkin method. Part III: Hybridized discontinuous Galerkin (HDG) formulation. Computers & Mathematics with Applications 75 (12), 4505–4533.

King, M.J., Dunayevski, V.A. (Eds.), 1989. Why waterflood works: A linearized stability analysis. Society of Petroleum Engineers.

Li, D., 1995. Scaling and upscaling of fluid flow through permeable media.

Lie, K.-A., 2019. An introduction to reservoir simulation using MATLAB/GNU Octave: User guide for the MATLAB reservoir simulation toolbox (MRST). Cambridge University Press, Cambridge, United Kingdom, New York, NY, USA, 1 Online-Ressource.

Lie, K.-A., Krogstad, S., Ligaarden, I.S., Natvig, J.R., Nilsen, H.M., Skaflestad, B., 2012. Open-source MATLAB implementation of consistent discretisations on complex grids. Comput Geosci 16 (2), 297–322. https://doi.org/10.1007/s10596-011-9244-4.

Mourlanette, P., Biver, P., Renard, P., Nœtinger, B., Caumon, G., Perrier, Y.A., 2020. Direct simulation of non-additive properties on unstructured grids. Advances in water resources 143, 103665. https://doi.org/10.1016/j.advwatres.2020.103665.

Noetinger, B., Artus, V., Ricard, L., 2004. Dynamics of the water–oil front for two-phase, immiscible flow in heterogeneous porous media. 2 – isotropic media. Transport in porous media 56 (3), 305–328. https://doi.org/10.1023/B:TIPM.0000026086.75908.ca.

Preux, C., 2016. About the use of quality indicators to reduce information loss when performing upscaling. Oil Gas Sci. Technol. – Rev. IFP Energies nouvelles 71 (1), 7. https://doi.org/10.2516/ogst/2014023.

Preux, C., Le Ravalec, M., Enchéry, G., 2016. Selecting an appropriate upscaled reservoir model based on connectivity analysis. Oil & Gas Science and Technology - Rev. IFP Energies nouvelles 71 (5), 60. https://doi.org/10.2516/ogst/2016015.

Quandalle, P., 1983. The use of flexible gridding for improved reservoir modeling, in: . SPE Reservoir Simulation Symposium. Society of Petroleum Engineers.

Reed, W.H., Hill, T.R., 1973. Triangular mesh methods for the neutron transport equation. Los Alamos Scientific Lab., N. Mex.(USA). https://www.osti.gov/servlets/purl/4491151.

Renard, P., Marsily, G. de, 1997. Calculating equivalent permeability: A review. Advances in water resources 20 (5-6), 253–278.

Reuter, B., Aizinger, V., Wieland, M., Frank, F., Knabner, P., 2016. FESTUNG: A MATLAB/GNU Octave toolbox for the discontinuous Galerkin method, Part II: Advection operator and slope limiting. Computers & Mathematics with Applications 72 (7), 1896–1925.

Reuter, B., Hajduk, H., Rupp, A., Frank, F., Aizinger, V., Knabner, P., 2020. FESTUNG 1.0: Overview, usage, and example applications of the MATLAB/GNU Octave toolbox for discontinuous Galerkin methods. Computers & Mathematics with Applications. https://doi.org/10.1016/j.camwa.2020.08.018.

Reuter, B., Rupp, A., Aizinger, V., Frank, F., Knabner, P., 2018. FESTUNG: A MATLAB/GNU Octave toolbox for the discontinuous Galerkin method. Part IV: Generic problem framework and model-coupling interface. arXiv preprint arXiv:1806.03908.

Riviere, B., 2008. Discontinuous Galerkin methods for solving elliptic and parabolic equations: Theory and implementation. SIAM.

Riviere, B., Wheeler, M.F., 2002. Discontinuous Galerkin methods for flow and transport problems in porous media. Commun. Numer. Meth. Engng. 18 (1), 63–68. https://doi.org/10.1002/cnm.464.

Riviere, B., Wheeler, M.F., Banaś, K., 2000. Part II. Discontinuous Galerkin method applied to a single phase flow in porous media. Computational Geosciences 4 (4), 337–349.

Schmidt, G., Jacobs, F., 1988. Adaptive local grid refinement and multi-grid in numerical reservoir simulation. Journal of Computational Physics 77 (1), 140–165. https://doi.org/10.1016/0021-9991(88)90160-x.

Sethian, J.A., 1996. A fast marching level set method for monotonically advancing fronts. Proceedings of the National Academy of Sciences 93 (4), 1591–1595.

Sorbie, K.S., Zhang, H.R., Tsibuklis, N.B., 1995. Linear viscous fingering: New experimental results, direct simulation and the evaluation of averaged models. Chemical Engineering Science 50 (4), 601–616. https://doi.org/10.1016/0009-2509(94)00252-M.

Spesivtsev, P., Teodorovich, E.V., 2007. The statistical characteristics of the displacement front in a randomly heterogeneous medium. Journal of Applied Mathematics and Mechanics 71 (3), 424–431. https://doi.org/10.1016/j.jappmathmech.2007.07.006.

Suslick, S.B., Schiozer, D.J., 2004. Risk analysis applied to petroleum exploration and production: an overview. Journal of Petroleum Science and Engineering 44 (1-2), 1–9. https://doi.org/10.1016/j.petrol.2004.02.001.

Tayari, F., Blumsack, S., Johns, R.T., Tham, S., Ghosh, S., 2018. Techno-economic assessment of reservoir heterogeneity and permeability variation on economic value of enhanced oil recovery by gas and foam flooding. Journal of Petroleum Science and Engineering 166, 913–923. https://doi.org/10.1016/j.petrol.2018.03.053.

Teodorovich, E.V., Spesivtsev, P.E., Nœtinger, B., 2011. A stochastic approach to the two-phase displacement problem in heterogeneous porous media. Transp Porous Med 87 (1), 151–177. https://doi.org/10.1007/s11242-010-9673-x.

Welge, H.J., 1952. A Simplified Method for Computing Oil Recovery by Gas or Water Drive. Journal of Petroleum Technology 4 (04), 91–98. https://doi.org/10.2118/124-G.

Wu, X.-H., Efendiev, Y., Hou, T.Y., 2002. Analysis of upscaling absolute permeability. Discrete and Continuous Dynamical Systems Series B 2 (2), 185–204.